RSC Advances

ROYAL SOCIETY OF CHEMISTRY

www.rsc.org/advances

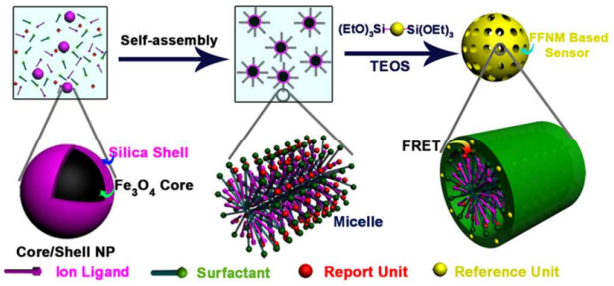

A magnetically recyclable ratiometric Cu^{2+} fluorescent sensor based on mesoporous silica nanoparticle was fabricated though a novel one-pot self-assembly method

Cite this: DOI: 10.1039/c0xx00000x

www.rsc.org/xxxxxx

Full paper

Self-Assembly of Magnetically Recoverable Ratiometric Cu^{2+} Fluorescent Sensor and Adsorbent

Deli Lu[a], Fei Teng[b], Yunchang Liu[a], Liujia Lu[a], Chen Chen[a], Juying Lei[a], Lingzhi Wang*[a], Jinlong Zhang*[a]

Received (in XXX, XXX) Xth XXXXXXXXX 20XX, Accepted Xth XXXXXXXXX 20XX
DOI: 10.1039/b000000x

Mesoporous shell containing fluorescence resonance energy transfer (FRET) type ratiometric Cu^{2+} fluorescent sensor was coated around a cetyltrimethylammonium bromide (CTAB) stabilized Fe_3O_4@SiO_2 core. All of units composed of the sensor composite including Cu^{2+} ligand, signal reference and report units are independent and without directly covalent linkage between them, which are site-selectively self-assembled into the pore framework or channel of mesoporous silica matrix through the electrostatic interaction between CTAB porogen and silicates. The coordination of Cu^{2+} and its ligand leads to the variation of fluorescence energy transfer efficiency between neighboring FRET pair benefited from the nanosized pore system of mesoporous matrix, which finally results in the ratiometric detection of Cu^{2+}. Investigation on Cu^{2+} adsorption performance indicated fast removal efficiency with maximum adsorption capacity of 17.86 mg/g. Fe_3O_4 NP was introduced as a core to make the sensor system magnetically recyclable after sensing and adsorption. Finally, the disassembly and reassembly of Cu^{2+} sensor were also achieved by extracting and reintroducing the units in CTAB micelle, making the sensing system reproducible.

Introduction

Surfactant chemistry has renewed its youth since the rise of nanomaterial science attributed to its indispensable role in stabilization of nanometer-sized metal or metal oxide and excellent performance on assembly of an all-in-one multifunctional system. A typical example is a core-shell type nanoparticle composed of a metal or metal oxide core and mesoporous shell, which is assembled from surfactant-stabilized core and surfactant-templated mesoporous shell. [1-4] In this system, surfactant perfectly plays the role of bridging two or more different functional units, which actually can be freely alternated according to the application purpose. Up to now, using core-shell NPs with mesoporous silica shell as examples, a library of nano-assembly NPs has been fabricated, for examples, Au@$mSiO_2$, Fe_3O_4@ $mSiO_2$, QD@$mSiO_2$, etc. [5-7] Besides its new application in nano-science, surfactant is traditionally recognized by its excellent ability on decreasing the surface tension and solubilization for hydrophobic organics.[8] For example, cloud point extraction technology adopting a system composed of surfactant and hydrophobic metal ion ligand is often used for the concentration and separation of metal ions.[9-11]

Here, with the help of artful combination of the old and new surfactant sciences, we develop a novel one-pot self-assembly method for the fabrication of magnetically recyclable ratiometric Cu^{2+} fluorescent sensor and adsorbent based on mesoporous silica. Fluorescent sensors are well-known for the advantages such as real-time, in site, convenience and accuracy, which have been elaborately designed and synthesized for the detection of ions and molecules in the fields of environment and biology.[12-19] However, they are obstructed for practical applications by disadvantages such as low sensitivity, complicated procedures for molecular fabrications and poor hydrophilicity.[20-26] Many efforts have been devoted to simplify the synthesis procedure and improve the sensing performance. For example, the detection sensitivity can be improved by combining organic sensor with nanoparticle due to the improved contact efficiency between sensor and target. [27-35]

However, the fabrication process, especially for ratiometric sensor is still complicated and needs multiple steps to covalently link different functional groups. It is still desirable to establish a more simple and convenient method for the sensor synthesis. We previously reported a pH ratiometric sensor by using mesoprous silica as the matrix and two commercially available fluorephores as signal reference and report units, where the detection sensitivity was greatly improved. [36] In this paper, we further developed a simple way for the fabrication of a multifunctional system assembling sensing, adsorption and magnetic recovery in one NP through artfully combining the old and new chemistry of surfactant. We adopted a CTAB stabilized Fe_3O_4@SiO_2 NP as the core and coated a fluorescent mesoporous shell around it, which was self-assembled through electrostatic force between cationic CTAB containing a Cu^{2+} ligand and fluorescein derivative and anionic silicates encapsulated with anthracene. All of units are just simply mixed in the synthesis system, and then ultimately select the sites they tend to dwell through an

autonomous way, which is actually driven by multiple forces including electrostatic, "like-dissolves-like" and silicates condensation. The basic purpose of this paper is to simplify the troublesome fabrication process of traditional fluorescent sensor and improve its detection performance by multifunctionalization with the aid of versatile surfactant chemistry, and then ultimately present a good example and means for the fabrication and assembly of novel materials.

Experimentals

1. Materials

Materials FITC and Bischloromethylanthracene were acquired from Amresco. $(Boc)_2O$, CF_3OOH, 1-Bromodecane and Glycine ethyl ester hydrochloride were supplied by Shanghai Kayon Biological Technology Co., Ltd.. CTAB, absolute ethanol, TEOS and ammonium hydroxide were purchased from Shanghai Sinopharm Chemical Reagent Co., Ltd., China. APTS was supplied by Shanghai Yaohua Chemical Plant. Distilled deionized water was used for the preparation of all aqueous solutions. All starting materials and solvents were used as received without further purification.

Preparation of bis-silylated Anth

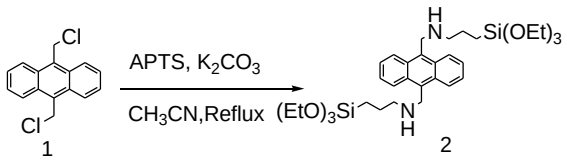

To a solution of 1 (0.548 g, 2 mmol) and K_2CO_3 (1.09 g, 8 mmol) in anhydrous CH_3CN (40 mL) solution, APTS (0.96 mL, 4 mmol) was added dropwise. The mixture was then heated to reflux for 48 h under N_2 atmosphere. After the reaction was completed, the solvent was removed under reduced pressure. The crude product was then purified by chromatography on a silica gel column (ethyl acetate) to give target product as a pale yellow liquid (192 mg, 15% yield); ^{1}H NMR (400 MHz $CDCl_3$) δ 0.68 (t, 4H, CH_2), 1.19 (t, 18H, CH_3), 1.68-1.74（m, 4H, CH_2), 2.54 (s, 2H, NH), 2.88 (t, 4H, CH_2), 3.79 (q, 12H, CH_2), 4.71 (s, 4H, CH_2), 7.52 (t, 4H, ArH), 8.38(d, 4H, ArH); ^{13}C NMR (100 MHz $CDCl_3$) δ: 8.05, 18.32, 23.39, 45.89, 53.43, 58.38, 124.94, 125.60, 126.46, 126.89, 127.59, 130.13, 132.20.

Preparation of Cu^{2+} ligand

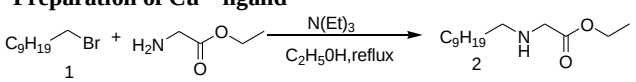

Preparation of intermediate 2 Glycine ethyl ester hydrochloride (8.84 g, 40 mmol) was added to a solution of the 1-bromodecane (8.84 g, 40 mmol) and triethylamine (2.75 mL, 19.6 mmol) in 50 mL of ethanol. The reaction mixture was refluxed for 6 h. After this time, the mixture was cooled to room temperature, 150 mL of $CHCl_3$ was added, and the organic phase was extracted with 0.5 M HCl (3 x 150 mL), a 10% $NaHCO_3$ solution (3 x 150 mL), and water (3 x 150 mL). The organic phase was dried (Na_2SO_4), and the solvent was evaporated. The crude product was purified by chromatography on a silica gel column (CH_2Cl_2) to give target product as a yellow liquid (2.4 g, 25% yield); ^{1}H NMR (400 MHz $CDCl_3$), δ: 0.88 (t, 3H, J = 3.2 Hz), 1.27 (t, 17H, J = 11.2 Hz), 1.49 (d, 2H, J = 5.6 Hz), 1.67 (s, 1H), 2.59 (m, 2H, J= 4 Hz), 3.39 (d, 2H, J = 6.4 Hz), 4.19 (m, 2H, J = 3.6 Hz); ^{13}C NMR (100 MHz, $CDCl_3$), δ: 14.13, 22.58, 27.16, 29.45, 29.99, 31.82, 49.58, 50.95, 60.52, 172.46.

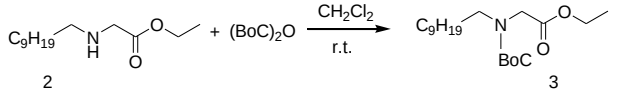

Preparation of intermediate 3 A solution of di-tert-butyl dicarbonate (1.89 g, 1.05 mmol) in 10 mL of $CHCl_3$ was added dropwise to a solution of the above N-alkylamino ester (2.2 g, 1 mmol) in 50 mL of $CHCl_3$. The reaction mixture was stirred at room temperature overnight, and then extracted with a 5% solution of Na_2CO_3. The organic phase was dried (Na_2SO_4), and the solvent was evaporated to yield the proper N-tert-butoxycarbonyl-N-alkylglycine ethyl ester as a yellow oil (2.99 g, 98% yield). ^{1}H NMR (400 MHz $CDCl_3$), δ: 0.88 (t, 3H, J = 3 Hz), 1.27 (t, 17H, J = 11.2 Hz), 1.43 (t, 4H, J = 2 Hz), 1.48 (d, 4H, J = 2 Hz), 1.53 (t, 3H, J = 2.8 Hz), 3.27 (m, 2H, J = 6.8 Hz); 13C NMR (100 MHz $CDCl_3$), δ: 14.04, 22.62, 26.73, 27.35, 28.26, 29.50, 31.84, 48.34, 48.69, 49.32, 60.84, 79.84, 170.14.

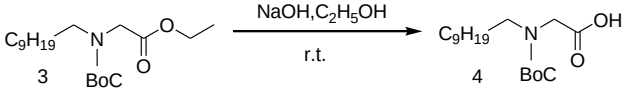

Preparation of intermediate 4 A 2 M solution of NaOH (10 mL, 20 mmol) was added to a solution of this Boc-protected derivative (0.72 g, 2 mmol) in MeOH (10 mL). The reaction mixture was stirred for 3 h at room temperature, and then the pH of solution was adjusted to about 7 with 1 M HCl, and the product was collected by filtration as a white solid (0.45 g, 99% yield). ^{1}H NMR (400 MHz $CDCl_3$), δ: 0.88 (t, 3H, J =6.8 Hz), 1.25 (s, 14H), 1.42 (s, 11H), 3.18 (t, 2H, J = 6.8 Hz), 3.61 (s, 2H); ^{13}C NMR (100 MHz $CDCl_3$), δ: 14.09, 22.68, 26.91, 28.41, 29.60, 31.94, 48.55, 51.46, 79.38, 156.97, 177.19.

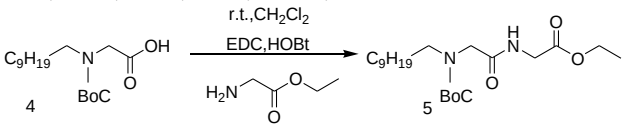

Preparation of intermediate 5 A solution of the above N-tert-butoxycarbonyl-N-alkylglycine (0.66g, 2 mmol) in CH_2Cl_2 was added to hydroxybenzotriazole (HOBt, 284 mg, 2.1 mmol), N-(3-dimethylaminopropyl)-N-ethylcarbodiimide (EDC, 402 mg, 2.1mmol), glycine ethyl ester hydrochloride (280 mg, 2 mmol) and triethylamine (280 μL, 2 mmol) in anhydrous CH_2Cl_2 (20 mL). The reaction mixture was stirred at room temperature overnight. After that, 30 mL of ethyl acetate was added, and the mixture was extracted with a 0.5 M citric acid solution (2 x 30 mL), a 5% $NaHCO_3$ solution (2 x 30 mL), and water (2 x 30 mL). The organic phase was dried with Na_2SO_4, and the solvent was removed to yield the proper protected N-alkyl dipeptide as a yellow oil (0.82 g, 99%) and without further purification for next step;^{1}H NMR (400 MHz $CDCl_3$), δ: 0.88 (t, 3H, J =6.8 Hz), 1.29 (t, 17H, J = 7 Hz), 1.47 (s, 8H), 1.53 (t, 3H, J = 7 Hz), 3.28 (t, 2H, J=7.4 Hz), 3.42 (s, 2H), 3.90 (s, 2H), 4.20 (m, 2H, J =7.2 Hz), 7.06 (s, 1H); 13C NMR (100 MHz $CDCl_3$), δ: 13.94, 22.52, 26.58, 28.11, 29.39, 31.74, 41.01, 50.04, 50.70, 61.23, 169.86.

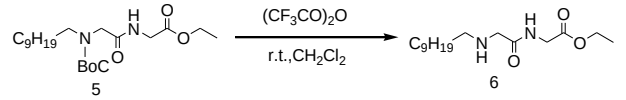

Preparation of intermediate 6 The protected N-alkyl dipeptide (0.83 g, 2 mmol) was dissolved in 10 mL of a 1:1 CH_2Cl_2/trifluoroacetic acid solution. The mixture was stirred at room temperature for 4 h, and then the pH was adjusted to 7 with a 10% Na_2CO_3 solution. The aqueous phase was extracted with $CHCl_3$ (5 x 10 mL), and the organic solution was dried, and the solvent was removed under vacuum. The crude product was purified by chromatography on a silica gel column (CH_2Cl_2) to give the product as a pale yellow liquid (0.79 g, 99% yield);^{1}H NMR (400 MHz $CDCl_3$), δ: 0.88 (t, 3H, J = 6.8 Hz)， 1.28 (m, 17H, J = 7.8 Hz), 1.72 (s, 2H), 3.06 (s, 2H), 3.16 (m, 1H, J = 3.0 Hz), 3.99 (s, 4H), 3.15 (m, 2H, J = 7.2 Hz), 8.75 (s, 1H); ^{13}C NMR (100 MHz $CDCl_3$), δ: 13.93, 22.58, 25.86, 26.43, 28.97, 29.26, 31.78, 41.18, 45.79, 48.19, 61.43, 80.41, 169.54.

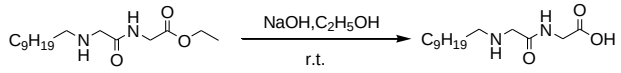

6 7

Preparation of target compound (Cu^{2+} ligand) A 2 M solution of NaOH (10 mL, 20 mmol) was added to a solution of compound 6 (0.8 g, 2 mmol) in MeOH (10 mL). The reaction mixture was stirred for 3 h at room temperature, and then the pH of solution was adjusted to about 7 with 1 M HCl, and the product was collected by filtration as a white solid (0.53 g, 99% yield). ^{1}H NMR (400 MHz D_2O), δ: 0.94 (t, 3H, CH_3), 1.38 (m, 14H, CH_2), 1.74 (m, 2H, CH_2), 3.07(t, 2H, CH_2), 3.88 (s, 2H, CH_2), 4.03 (s, 2H, CH_2); ^{13}C NMR (100 MHz D_2O), δ: 13.93, 22.58, 25.86, 26.43, 28.97, 29.26, 31.78, 41.18, 45.79, 48.19, 80.41, 169.54.

Preparation of fluorescent reporter unit

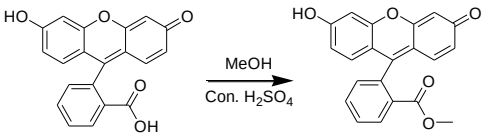

Preparation of fluorescein methyl ester Concentrated H_2SO_4 (2.5 mL) was added dropwise to a suspension of fluorescein (3.32 g, 10 mmol) in methanol (10 mL) and the resulted suspension was refluxed for 14 h. The mixture was then cooled and ice (3 g) followed by $NaHCO_3$ (10 g) was added. The suspension was filtered and washed with water and 2% $NaHCO_3$ solution for three times, respectively. The obtained pellet was resuspended in 1% acetic acid, filtered, washed with water, and finally dried at 110 ^{o}C for 1 h, to give a red powder (3.3 g, 95% yield) without further purification for next step. ^{1}H NMR (400 MHz $CDCl_3$) δ: 3.94 (s, 3H, CH_3), 5.21 (s, 1H, OH), 6.798 (d, 2H, ArHz), 6.79 (d, 2H, ArH), 7.30 (d, 2H, ArH), 7.65 (d, 1H, ArH), 7.66 (t, 1H, ArH), 7.71 (t, 1H, ArH), 8.23 (d, 1H, ArH).

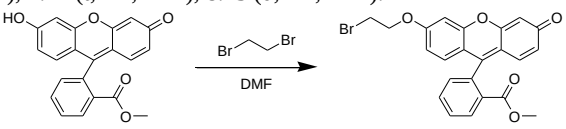

Preparation of fluorescent reporter unit A mixture of ethylene dibromide (197 mg, 91 μL, 1.05 momol), K_2CO_3 (288 mg, 2.1 mmol) and N,N-dimethylformamide (DMF, 10 mL) was added the fluorescein methyl ester (345 mg ,1 mmol), and heated to 60 ^{o}C for 3 h. After that, saturated NaCl solution (40 mL) was added to precipitate. The filtered recipitate was washed with water, 1% NaOH solution and water, and finally dried to yield orange powder without further purification for next step (443 mg, yield 90%). ^{1}H NMR (400 MHz $CDCl_3$) δ: 3.65 (s, 3H, CH_3), 3.68 (t, 2H, CH_2), 4.40 (t, 2H, CH_2), 6.45 (s, 1H, ArH), 6.54 (d, 2H, ArH), 6.75 (d, 1H, ArH), 6.84 (d 1H, ArH), 6.90 (d, 1H, ArH), 6.95 (s, 1H, ArH), 7.31 (d, 1H, ArH), 7.67 (t, 1H, ArH), 7.74 (t, 1H, ArH), 8.25 (d, 1H, ArH); ^{13}C NMR (100 MHz $CDCl_3$) δ: 28.25, 52,44, 68.33, 101.11, 155.88, 113.53, 115.36, 117.91, 129,03, 129.75, 130.05, 130.24, 131.18, 132.75, 134.56, 149.94, 154.1, 158.89, 162.31, 165.58.

Synthesis of Fe_3O_4 particles $FeCl_3$ $6H_2O$ (0.85 g), trisodium citrate dehydrate (0.48 g), and sodium acetate (1.75 g) were dissolved in ethylene glycol (30 mL) under magnetic stirring. The obtained homogeneous yellow solution was transferred to a Teflon-lined stainless-steel autoclave with a capacity of 40 mL. The autoclave was heated to 200 ℃ and maintained for 10 h, and then, it was cooled down to room temperature. The obtained black magnetite particles were washed with water and ethanol for five times. The particles were conserved in the ethanol.

Preparation of Core−Shell Fe_3O_4@nSiO_2 particles Typically, the Fe_3O_4 particles (40 mg) were dispersed in an ethanol (200 mL) and water (50 mL) solution. Followed by the addition of ammonia aqueous solution (3.0 mL, 25 wt %) and TEOS (200 μL). After stirring at 25 °C for 10 h, the Fe_3O_4@nSiO_2 spheres were obtained and washed three times with water and ethanol, respectively.

Preparation of core−shell Fe_3O_4@nSiO_2@mSiO_2 spheres Typically, the Fe_3O_4@nSiO_2 particles (10 mg) were dispersed in an ethanol (10 mL) and water (30 mL) solution containing 75 mg CTAB. Followed by the addition of ammonia aqueous solution (0.27 mL, 25 wt %), TEOS (100 μL) and bis-silylated anthracene (10 μL). After stirring at 25 ℃ for 10 h, the Fe_3O_4@nSiO_2@mSiO_2 spheres were obtained and washed three times with water and ethanol, respectively.

Preparation of Cu^{2+} fluorescent sensor using Fe_3O_4@nSiO_2 NP as the core The magnetically recoverable sensor system was prepared by the same procedure with anthracene contained Fe_3O_4@nSiO_2@mSiO_2 except by mixing fluorescein derivative and the ligand in the CTAB ethanol and water solution before the addition of silica source.

Influence of pH value to the fluorescence emission of sensor system The pH value of fluorescent sensor solution was adjusted using different buffer solutions. The specific operation was as follows: (1) Preparation of a series of aqueous solution with various pH values from 2 to 12 using different buffer solutions; (2) 100 μg FFNM was added to the above solutions (5 mL) and the fluorescent intensity was recorded after equilibrium for 5 min.

Cu^{2+} detection The detection procedure was as follows: (1) Preparation of 50 μg mL^{-1} Hepes buffer aqueous solution (50 mM, pH=7.2) of Cu^{2+} sensor; (2) Different amount of Cu^{2+} was added to a solution of FFNM based Cu^{2+} sensor (3 mL), and the fluorescent intensity was recorded after equilibrium for 5 min.

Adsorption of Cu^{2+} The experiments of adsorption isotherms were conducted as follows: 2 mg of FFNM was added into a solution was equilibrated with various concentrations of Cu^{2+} (10 mL). The concentrations of the Cu^{2+} ranged from 1 to 30 mg L^{-1} with the initial pH of 7.0.

Disassembly and reassembly of Cu^{2+} sensor FFNM based Cu^{2+} sensor was dispersed in ethanol for 1 h, then washed with water and magnetically recovered. The disassembly is verified by

investigating the I_{540}/I_{425} ratio. The reassembly is achieved by dispersing FFNM particle into a 5% EtOH water solution containing the ligand and fluorescein, where the addition of small amount of EtOH is to ensure the dissolution of hydrophobic ligand and fluorescein in water solution.

4. Characterization

X-ray powder diffraction (XRD) patterns of all samples were recorded on Rigaku D/MAX-2550 diffractometer using Cu Kα radiation on wavelength of 0.154 nm, operated at 40 kV and 100 mA. UV-visible absorbance spectra were obtained with a scan UV-visible spectrophotometer (Varian, Cary 500). The fluorescence spectra of all samples were recorded with Cary Eclipse fluorescence spectrophotometer. Scanning electron microscopy (SEM) images were obtained with a JEOL JSM-6360LV microscope at an accelerating voltage of 15 kV. Transmission electron microscopy (TEM) images were collected on a JEOL JEM 2010F, and the electron microscope was operated at an acceleration voltage of 200 kV. ^{1}H and ^{13}C NMR spectra were obtained on a Bruker AVANCE DMX500 spectrometer in $CDCl_3$ with tetramethylsilane (TMS) as internal standard. Electron impact mass spectra were recorded on an Agilent 5973N MSD instrument, and ESI mass spectra were recorded on Agilent 11100-Finnigan instrument. The Zn^{2+} concentrations were recorded on Varian-710-ES instrument with ICP/AES data.

Results and discussions

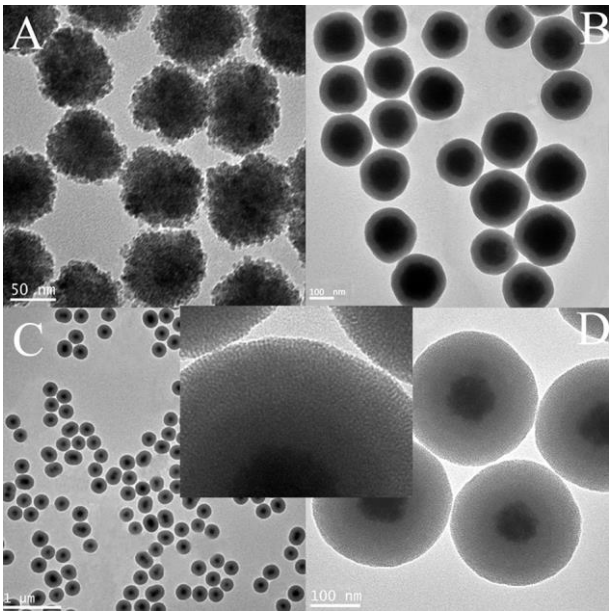

Fig. 1 Fe_3O_4 nanoparticle (A), Fe_3O_4@$nSiO_2$ particle (B) and fluorescent Fe_3O_4@$nSiO_2$@$mSiO_2$ particle (C and D). Insert is the enlargement of the mesoporous shell.

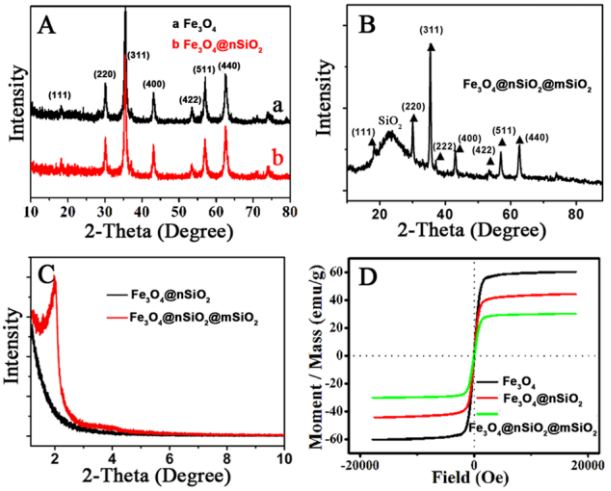

Fig. 2 Wide XRD patterns of Fe_3O_4 and Fe_3O_4@$nSiO_2$ (A), wide XRD pattern of Fe_3O_4@$nSiO_2$@$mSiO_2$ (B), small angle XRD patterns of Fe_3O_4@$nSiO_2$ and Fe_3O_4@$nSiO_2$@$mSiO_2$(C) , and magnetization hysteresis loops of Fe_3O_4, Fe_3O_4@$nSiO_2$ and Fe_3O_4@$nSiO_2$@$mSiO_2$ (D), respectively.

Mesoporous and magnetic characteristics of fluorescent Fe_3O_4@$nSiO_2$@$mSiO_2$ (FFNM) Fig. 1 shows TEM images of iron oxide nanoparticles before (A) and after coatings of

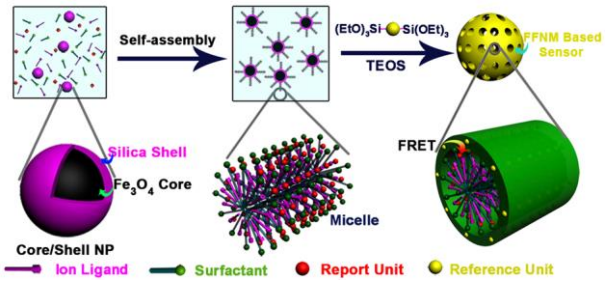

Scheme 1 Ratiometric fluorescent sensor composed of signal reference unit, signal report unit and ligand unit through the formation process of mesoporous silica.

unonporous inner silica layer (B, $nSiO_2$) and mesoporous outer silica layer (C and D, $mSiO_2$). The diameter of iron oxide nanoparticle is about 100 nm and the radii of amorphous and mesoporous silica layers are about 35 nm and 50 nm, respectively, where all of particles are highly dispersed. The mesoporous pore system diverges from the center to the fringes (Insert of Fig. 1) and has hexagonal mesopore symmetry (Fig. 2 C) revealed by HRTEM and small angle XRD pattern, respectively. The wide XRD pattern of FFNM indicates the iron oxide core is superparamagnetic Fe_3O_4, and magnetization saturation values of Fe_3O_4, Fe_3O_4@$nSiO_2$ and Fe_3O_4@$nSiO_2$@$mSiO_2$ are 60, 40 and 30 emu/g, respectively (Fig.2 A, B and D). No remanence is detected for all of samples according to the hysteresis loop, further confirming the superparamagnetism of these particles.

Self-assembly of Cu^{2+} fluorescent sensor Scheme 1 shows the assembly process of Cu^{2+} ligand, signal reference and report units into mesoporous shell using CTAB stabilized Fe_3O_4@$nSiO_2$ NP as the core. We chose bis-silylated anthracene [37]and fluorescein derivative as the signal reference and report units, which are the energy donor and acceptor of an FRET pair and finally dwell in the silicates wall and CTAB occupied pore channel after the formation of mesoporous matrix through the electrostatic

interaction between cationic surfactant and anionic silicates. Glycylglycine dipeptide is used as the ligand unit, [38] and dwell in hydrophobic micelle with fluorescein derivative attributed to the "like dissolves like" principle. This system functions as Cu^{2+} ratiometric sensor through the complex between Cu^{2+} and its ligand and their influence to the FRET process of anthracene-fluorescein pair (Scheme 2). The traditional synthesis of a FRET type ratiometric sensor requires the covalent linkage between energy donor and acceptor to achieve the effective energy transfer. However, in this system, the covalent linkage between donor and acceptor becomes unnecessary and even the covalent linkage between ligand and fluorephore is avoided, which are benefited from effectively shortened distance between different units confined in the nanometer-sized pore system since the unit cell parameter of the mesoporous shell is only 4.5 nm.

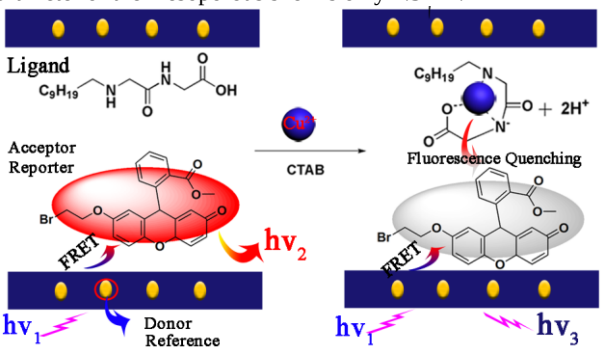

Scheme 2 Molecular structures of Cu^{2+} ligand, fluorescent report unit and the probable FRET response mechanism to Cu^{2+}.

Sensing selectivity to Cu^{2+} Fig. 3 shows the emission and excitation spectra of anthracene and fluorescein derivative, where the emission spectrum of anthracene and the absorption spectrum of fluorescein have a good overlap, making them possible to form FRET. When the composite assembled from anthracene and fluorescein is excited at 370 nm, where anthracene has obvious absorption while fluorescein has negligible absorption, both the emissions of anthracene and fluorescein are observed (Fig. 4 A). The above results indicate that an effective FRET process happens between anthracene and fluorescein even without covalent linkage.

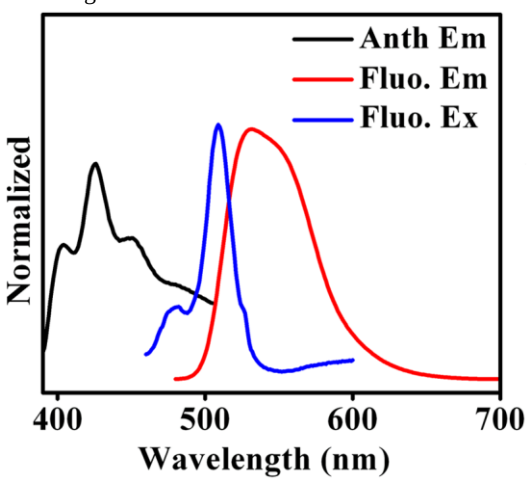

Figure 3. Emission and excitation spectra of anthracene and fluorescein derivative.

Fig.4 shows the fluorescence spectra of FFNM based Cu^{2+} sensor prepared with different amounts of report unit. The fluorescein concentration is finally fixed at $2x10^{-7}$ mol for the subsequent study in consideration of the fluorescence self-quenching caused by the over high molecule concentration (Fig. 4 A). Fig. 4 B shows the ratiometric (I_{540}/I_{425}) fluorescence response to the variation of pH value, where I_{540} and I_{425} refer

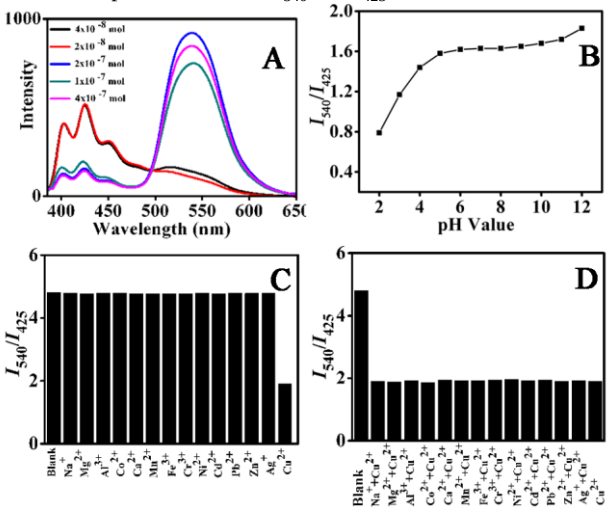

Fig. 4 (A) Fluorescence spectra of FFNM based Cu^{2+} sensor prepared with different amounts of report unit; (B) Fluorescence intensity ratios between report and reference dyes plotted as I_{540}/I_{425} under various pH values; (C) Responses of sensor to different metal ions (50 μM) and (D) Fluorescent response of sensor in the presence of 10 μM Cu^{2+} and various metal ions (50 μM) (λ_{Ex}=370 nm, λ_{Em} = 425 and 540 nm).

to the intensity of fluorescein and anthracene, respectively. It is found that the I_{540}/I_{425} value remains nearly unaffected in the pH range of 6 to 10. The sudden decrease from 5 to 2 should be resulted from the protonation of fluorescein derivative. Therefore, for the subsequent studies, we fixed the pH value at 7.2 using HEPES buffer solution (20 mM). Fig. 4 C shows ratiometric (I_{540}/I_{425}) fluorescence variation of sensor in the presence of various metal ions. It can be found that the I_{540}/I_{425} value dramatically decreases after the addition of Cu^{2+} (10^{-5} M). However, the addition of other metal ions such as Fe^{3+}, Pb^{2+}, Cd^{2+} and Ag^{+} results in a negligible change. Fig. 4 D shows the interference of other ions such as Li^{+}, Na^{+}, K^{+}, Mg^{2+}, Ca^{2+}, Fe^{2+}, Co^{2+}, Ni^{2+}, Zn^{2+}, Cd^{2+}, Ag^{+}, and Pb^{2+} (10^{-4} M) to the I_{540}/I_{425} value in the presence of Cu^{2+} (10^{-5} M). No significant variation of I_{540}/I_{425} is observed compared with the blank sample only added with Cu^{2+}, which indicates that this system has an excellent selective detection performance to Cu^{2+}.

Sensitivity of sensor to Cu^{2+} Subsequently, the sensitivity of the above sensor to Cu^{2+} is investigated as shown in Figure 5. It is evident that the emission of the report unit at 540 nm gradually decreases with the increasing Cu^{2+} concentration

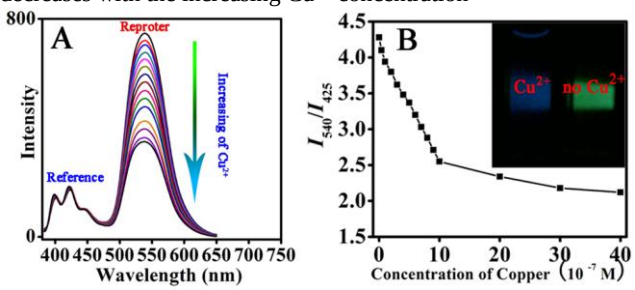

Fig. 5 (A) Fluorescent spectra of sensor with different amounts of Cu^{2+}; (B) Ratiometric calibration curve (I_{540}/I_{425}) as a function of Cu^{2+} concentration (Insert: Imaging of sensor solution before and after the addition of Cu^{2+})

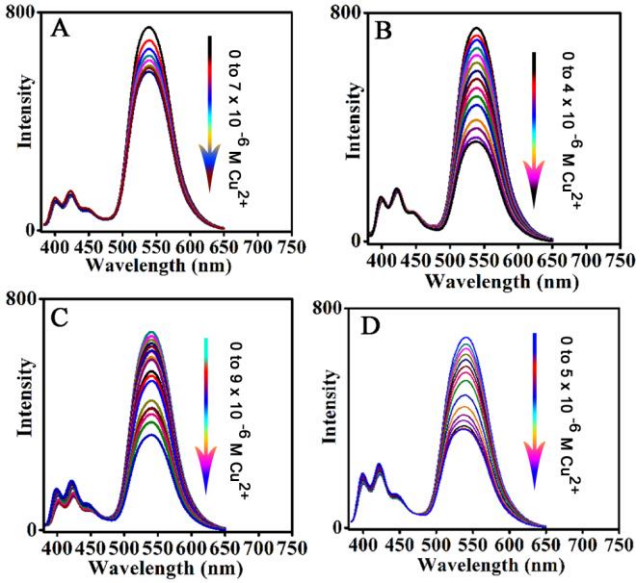

Fig. 6 The effect of loading amount of fluorescence signal reporter and Cu^{2+} receptor on the detection sensitivity. (A: ligand (0.1 mL, $3x10^{-4}$ M), fluorescent reporter (1 mL, $2x10^{-4}$ M); B: ligand (2 mL, $3x10^{-4}$ M), fluorescent reporter (1 mL, $2x10^{-4}$ M); C: ligand (4 mL, $3x10^{-4}$ M), fluorescent reporter (1 mL, $2x10^{-4}$ M); D: fluorescent reporter (2 mL, $2x10^{-4}$ M), ligand (2 mL, $3x10^{-4}$ M).

from 0 to 6 x 10^{-6} M (Fig. 5 A). The detection limit is 5 x 10^{-8} M by setting the confidence level at 3, which indicates the sensor is highly sensitive. On the contrary, the reference unit shows a stable emission signal, which is hardly affected by the variation of Cu^{2+} concentration and should be attributed to the protection from the framework shell since the encapsulation of anthracene molecules make them isolating from surrounding environment.

The fluorescence before and after the addition of Cu^{2+} can be clearly observed by naked-eye under UV light irradiation as shown in Fig. 5 B.The above sensor system with excellent sensing performance are carefully chosen from FFNM particle loaded with different amounts of report and ligand units, which are prepared with $2x10^{-7}$ mol of ligand and $6x10^{-7}$ mol of signal report units (Fig. 6 B). Lower and higher amounts of ligand actually lead to the decreased sensitivity. The lower sensitivity of the system with less amount of receptor ($3x10^{-8}$ mol, Fig. 6 A) should be attributed to the ineffective influence of coordinated Cu^{2+} to remote fluorephores since the inhomogeneous distribution of tiny amount of receptor units in the pore channel, while the lower sensitivity of the system with higher amount of ligand ($1.2x10^{-6}$ mol, Fig. 6 C) should be attributed to the part isolation of coordinated Cu^{2+} surrounded by excessive complex units from neighboring fluorephores. Moreover, it is also noted that excessive amounts of report unit (Fig. 6 D) would also result in the decreasing of detection sensitivity due to the increasing self-quenching caused by high concentrated fluorephore.

Adsorption performance Besides the sensing performance, we also investigated the adsorption capacity of FFNM sensor for

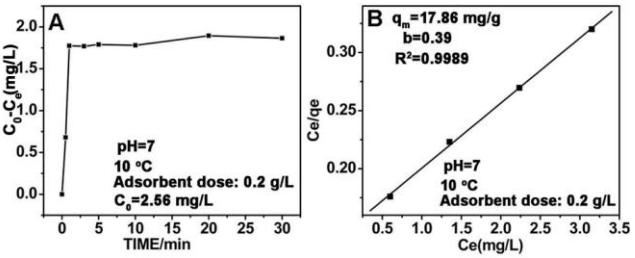

Fig. 7 Adsorption kinetics curve (A) and Langmuir isotherm curve for the adsorption of Cu^{2+} by FFNM sensor (B).

Cu^{2+} calculated according to mass balance for Cu^{2+} ion expressed as equation 1, where q_e is adsorption capacity (mg g^{-1}), C_0 and C_e are the initial and equilibrium concentrations of Cu^{2+} ions (mg L^{-1}), M is the mass of FFNM (g), and V is the volume of added solution (L).

$$q_e = \frac{(C_0 - C_e) \times V}{M} \quad (1)$$

$$C_e/q_e = 1/bq_m + C_e/q_m \quad (2)$$

Fig. 7 A shows the adsorption kinetic curve of FFNM based sensor. It can be found that the uptake of Cu^{2+} by FFNM particle is a very fast process, which finishes in 1 min. This fast process is attributed to the porous structure of FFNM and strong affinity of the glycylglycine dipeptide ligand to Cu^{2+}. The adsorption capacity of FFNM for Cu^{2+} was investigated at different initial metal concentration (1-30 mg L^{-1}). The adsorption equilibrium data were fitted by the Langmuir adsorption isotherm model as seen from equation 2, where C_e, q_e, b and q_m are equilibrium solution concentration (mg L^{-1}), equilibrium adsorption capacity (mg g^{-1}), Langmuir adsorption equilibrium constant (L mg^{-1}) and maximum adsorption capacity (mg g^{-1}), respectively. The experimental adsorption data were fitted with the Langmuir isotherm equation and is shown in Fig. 7 B. It can be seen that the value of b and q_m is 0.39 L mg^{-1} and 17.86 mg g^{-1}, respectively. The R value of 0.9989 means that the adsorption process can be well described by the Langmuir adsorption isotherm, which is dependent on the amount of the available adsorption sites on the pore surface of the adsorbent.

Magnetic response and recycling sensing performance As illustrated above, the FFNM particle is supermagnetic with a saturation magnetization value of 30 emu g^{-1}, which can be fast separated from water within 1 min when a magnet was placed near the glass bottle (Fig. 8 B). This result indicates that the FFNM particle can be easily recovered by adding an external magnetic field after the sensing and adsorption of Cu^{2+}.

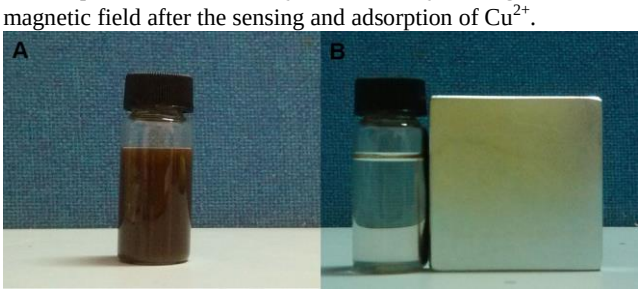

Fig. 8 Water solution of FFNM particle (A) and its magnetic separation (B).

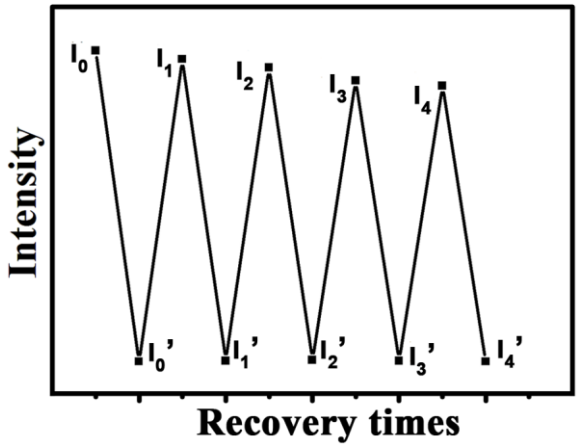

Fig. 9 Reversibility of the fluorescence sensing performance of FFNM to Cu^{2+} (2 x 10^{-4} mol) after the disassembly and reassembly of sensor system. I_0 and I_0' refer to the original I_{540}/I_{425} ratio before and after coordinated with Cu^{2+}. I_1~I_4 correspond to the I_{540}/I_{425} ratio after the disassembly-resassembly process. $I_{1'}$~$I_{4'}$ corresponds to the fluorescence intensity of FFNM after reassembly and coordinated with Cu^{2+}.

Subsequently, the recycling sensing performance of FFNM based sensor was further studied through a disassembly and reassembly process. After the recycling of FFNM by magnetic force, the ligand and signal report units in CTAB micelle were extracted by redispersing FFNM particle in ethanol. The complete extraction is verified by the disappearance of the fluorescence signal of the report unit. The I_{540}/I_{425} value and the sensing ability to Cu^{2+} can be recovered by dispersing the particle in a 5% ethanol water solution containing signal report unit and the ligand, where the addition of small amount of EtOH is to ensure the dissolution of hydrophobic ligand and fluorescein derivative in water solution. After repeated for 4 cycles, this particle still preserves 90% of original I_{540}/I_{425} value and its sensing ability to Cu^{2+} (Fig. 9). The loss of the fluorescence intensity should be attributed to the loss of CTAB from the pore channel during the ethanol extraction process, leading to the decreasing of the enrichment ability for ligand and fluorescein.

Conclusions

In conclusion, we present a novel self-assembly route for the fabrication of FRET type ratiometric fluorescent sensor by integrating the preparation process of sensor into the one-pot formation process of core-shell mesoporous silica using CTAB stabilized Fe_3O_4@nSiO_2 as the core, where all of the units composing the sensor are elaborately arranged in the different area of mesoporous matrix and can effectively interact with each other even without directly covalent linkage between them. This nanocomposite system provides a robust platform for the design of novel materials through appropriately utilizing the versatile surfactant chemistry. In this paper, the fabrication and multifunctionalization of ratiometric fluorescent sensor process is significantly simplified and no effort needs to be paid on covalent bonding of different sensor units, which should be flexible and variable depending on the detection target.

Acknowledgements

This work has been supported by the National Nature Science Foundation of China (21173077, and 21237003); the National Basic Research Program of China (973 Program, 2013CB632403); the Project of International Cooperation of the Ministry of Science and Technology of China (No. 2011DFA50530); Science and Technology Commission of Shanghai Municipality (12230705000, 12XD1402200); the Research Fund for the Doctoral Program of Higher Education(20120074130001). Open Project from Jiangsu Key Laboratory of Atmospheric Environment Monitoring and Pollution Control of Nanjing University of Information Science and Technology (kHK1110), Jiangsu Province Innovation Platform for Superiority Subject of Environmental Science and Engineering.

Notes and References

[a] *Key Lab for Advanced materials and Institute of Fine Chemicals,East China University of Science and Technology, Shanghai 200237 (P. R. China), E-mail: wlz@ecust.edu.cn and jlzhang@ecust.edu.cn,Fax: (+86) 021-6425 2062*
[b] *Innovative Research Laboratory of Environment & Energy, Jiangsu Key Laboratory of Atmospheric Environment Monitoring & Pollution Control, School of Environmental Science and Engineering, Nanjing University of Information Science & Technology*

† Electronic Supplementary Information (ESI) available: See DOI: 10.1039/b000000x/

1 V. Cauda, A. Schlossbauer, J. Kecht, A. Zurner and T. Bein, J. Am. Chem. Soc., 2009, 131, 11361.
2 G. Büchel, K. Unger, A. Matsumoton, and K. Tsutsumi, *Adv. Mater.*, 1998, **10**, 1036.
3 W. Zhao, J. Gu, L. Zhang, H. Chen and J. Shi, *J. Am. Chem. Soc.*, 2005, **127**, 8916.
4 F. Wang, X. L. Chen, Z. X. Zhao, S. H. Tang, X. Q. Huang, C. H. Lin, C. B. Cai, and N. F. Zheng, *J. Mater. Chem.*, 2011, **21**, 11244.
5 H. Lim and S. Lippard, *Acc. Chem. Res.*, 2007, **40**, 41.
6 C. Yang, X. Sun and B. Liu, *Analytica Chimica Acta*, 2012, **746**, 90.
7 Z. Jiang, X. Li, G. Yang, L. Cheng, B. Cai, Y. Yang, and J. Dong, *Langmuir*, 2012, **28**, 7174.
8 L. Zhao, S. Zhong, K. Fang, and Q. Chen, *Journal of Hazardous Materials*, 2012, **239-240**, 206.
9 C. Sahin, M. Efecinar, and S. Nuray. *Journal of Hazardous Materials*, 2010, **176**, 672.
10 M. Luconi, R. Olsina, L. Fernandez, M. Silva, *Journal of Hazardous Materials*, 2006, **128**, 240.
11 A. P. De Silva, H. Q. N. Gunaratne, T. Gunnlaugsson, A. J. M. Huxley, C. P. McCoy, J. T. Rademacher, and T. E. Rice, *Chem. Rev.*, 1997, **97**, 1515.
12 J. F. Zhang, Y. Zhou, J. Y. Yoon, Y. Kim, S. J. Kim, and J. S. Kim, *Org. Lett.*, 2010, **12**, 3852.
13 D. Buccella, J. A. Horowitz, and S. J. Lippard, *J. Am. Chem. Soc.*, 2011, **133**, 4101.
14 K. Hanaoka, Y. Muramatsu, U. Yasuteru; T. Terai, and T. Nagano, Chem. Eur. J., 2010, 16, 568.
15 R. H. Yang, W. H. Chan, A. W. M. Lee, P. F. Xia; H. K. Zhang, K. A. Li, *J. Am. Chem. Soc.*, 2003, **125**, 2884.
16 B. C. Zhu, F. Yuan, R. X. Li, Y. M. Li, Q. Wei, Z. M. Ma, B. Du and X. L. Zhang, *Chem. Commun.*, 2011, **47**, 7098.

17 X. L. Zhang, Y. Xiao and X. H. Qian, *Angew. Chem. Int. Ed.*, 2008, **47**, 8025.

18 S. C. Burdette, C. J. Frederickson, W. W. Bu and S. J. Lippard, *J. Am. Chem. Soc*., 2003, **125**, 1778.

19 Z. P. Liu, W. J. He, and Z. J. Guo, *Chem. Soc. Rev.*, 2013,**42**, 1568.

20 E. M. Nolan, J. Jaworski, K. Okamoto, Y. Hayashi, M. Sheng, and S. J. Lippard, *J. Am. Chem. Soc.* 2005, **127**, 16812.

21 Z. Xu, K. Baek, H. N. Kim, J. N. Cui, X. H. Qian, D. R. Spring, I. Shin and J. Yoon, *J. Am. Chem. Soc.*, 2010, **132**, 601.

22 A. Coskun, and E. Akkaya, *J. Am. Chem. Soc.*, 2006, **128**, 14474.

23 K. Komatsu, Y. Urano, H. Kojima and T. Nagano, *J. Am. Chem. Soc.*, 2007, **129**, 13447.

24 A. Mokhir, A. Kiel, D. Herten, and R. Kraemer, *Inorganic Chemistry*, 2005, **44**, 5661.

25 K. M. K. Swamy, S. Ko, S. K. Kwon, H. N. Lee, C. Mao, J. M. Kim, K. Lee, J. Kim, I. Shin and J. Y. Yoon, *Chem. Commun.* 2008, 5915.

26 L. X. Yan, Z. P. Chen, Z. Y. Zhang, C. G. Qu, L. X. Chen and D. Z. Shen, *Analyst*, 2013, **138**, 4280.

27 P. T. Snee, R. C. Somers, G. J. Nair, P. M. Zimmer, G. D. Bawendi, and G. Nocera, *J. Am. Chem. Soc.*, 2006, **128**, 13320.

28 M. Frigoli, K. Ouadahi and C. Larpent, *Chem. Eur. J.*, 2009, **15**, 8319.

29 B. Paramanik, S. Bhattacharyya and A. Patra, *Chem. Eur. J.*, 2013, **19**, 5980.

30 B. D. Wang, J. Hai, Z. C. Liu, Q. Wang, Z. Y. Yang, and S. H. Sun, *Angew. Chem. Int. Ed.*, 2010, **49**, 4576.

31 H. J. Son, H. Y. Lee, J. M. Lim, D. M. Kang, W. S. S. Han, S. J. Lee, and H. Jung, *Chem. Eur. J.*, 2010, **16**, 11549.

32 Q. T. Meng, X. L. Zhang, C. He, G. J. He, P. Zhou and C. Y. Duan, *Adv. Funct. Mater.*, 2010, **20**, 1903.

33 J. L. Liu, C. Y. Li, and F. Y. Li, *J. Mater. Chem.*, 2011, **21**, 7175.

34 L. X. Mu, W. S. Shi, J. C. Chang, *Nano Lett.*, 2008, **8**, 104.

35 X. H. Peng, Y. J. Wang, X. L. Tang and W. S. Liu, *Dyes and Pigments*, 2011, **91**, 26.

36 L. Z. Wang, J. Y. Lei and J. L. Zhang, *Chem. Commun.*, 2009, **16**, 2195.

37 D. L. Lu, J. Y. Lei, L. Z. Wang and J. L. Zhang, *J. Am. Chem. Soc.*, 2012, **134**, 8746.

38 P. Grandini, F. Mancin, P. Tecilla, P. Scrimin, and U. Tonellato, *Angew. Chem. Int. Ed.*, 1999, **38**, 3061.